波 谱 学 杂 志

第32卷第2期 Vol. 32 No. 2
2015年06月 Chinese Journal of Magnetic Resonance Jun. 2015

Article: 1000-4556(2015)02-308-10 doi:10.11938/cjmr20150213

The Extended Loop Reduces Ca^{2+}-Binding Affinity on the Tellurite Resistance Protein TerZ from *Klebsiella penumoniae*

WEI Shu-yi, *PAN Yun-ru*, *TSENG Tien-sheng*, *CHEN Chin-pan**

(Institute of Biomedical Sciences, "Academia Sinica", Taipei 11529)

Abstract: Tellurite (TeO_3^{2-}), an oxyanion of tellurium, is highly toxic to most microorganisms. Several tellurite resistance genes (*terZABCDEF*) have been identified in many pathogenic bacteria. Previously, we determined the NMR solution structure of the tellurite resistance protein TerD and suggested that TerD may function as a calcium sensor in bacteria. TerZ, which shares 40% sequence identity with TerD, contains an extra 9-residue segment of $L_{36}FGSIFGGN_{44}$ and exhibits much weaker Ca^{2+}-binding affinity. Interestingly, $TerZ_{del}$ in which the extra segment is deleted has comparable binding affinity to TerD. Based on chemical shift index and homology modeling results, it was revealed that the extra segment is unstructured and forms an extended loop, which may disturb the conformation of Ca^{2+}-binding sites and also prevent Ca^{2+} from contacting its binding site, hence significantly reduce Ca^{2+}-binding affinity.

Key words: Ca^{2+}-binding protein, tellurite resistance, calcium sensor, chemical shift index, homology modeling

CLC number: O482.53 **Document code:** A

Introduction

Oxyanions of tellurium, tellurite (TeO_3^{2-}) and tellurate (TeO_4^{2-}), are highly toxic to most microorganisms[1,2]. Genes associated with tellurite resistance (Te^R) are found in many pathogenic bacteria and are mostly conferred by highly specific genetic determinants[3]. For example, a gene cluster encoding an *E. coli* (*Escherichia coli*) *terZABCDE* homolog was identified in the large virulence plasmid pLVPK of *K. pneumoniae* CG43, the major cause of

Received date: 2015-03-02; **Revised date:** 2015-05-08

Foundation item: "Academia Sinica and the National Science Council" (NSC103-2311-B-001-026-MY3).

Biography: *Corresponding author: CHEN Chin-pan, Tel: +886-2-27899162, E-mail: bmchinp@ibms.sinica.tw.

community-acquired pyogenic infections[4]. In addition to conferring tellurite resistance, this gene cluster also provides resistance against infection by bacteriophages and pore-forming colicins[5]. Recently, the mutual association of tellurite resistance proteins in the inner plasma membrane and the cytosol was found responsible for their function[6], and Ter-dependent stress systems are related to metal sensing and DNA-processing[7]. However, most of the proteins involved in Te^R have no similarities with any other known proteins, which cause difficulties in understanding how they function. Therefore, the mechanism underlying tellurite resistance is still poorly understood.

Previously, we solved the 3D NMR structure of the tellurite resistance TerD protein of *K. pneumoniae*, which binds 2 Ca^{2+} ions with distinct binding affinities[8]. Intriguingly, one of the Ca^{2+}-binding affinities (~200 nmol/L) is in the ideal range to function as a calcium sensor in bacteria. The 2 Ca^{2+}-binding sites are highly conserved in TerD proteins among a wide range of bacterial species and are also likely to be represented in the other 2 tellurite resistance proteins, TerE and TerZ, both with identical Ca^{2+}-binding residues as TerD (Fig. 1). Using EDTA titration by one-dimensional NMR, we found that both TerE and TerZ are indeed Ca^{2+}-binding proteins. However, Ca^{2+}-binding affinity on TerZ, which shares 40% sequence identity to TerD and contains an extra 9-residue segment of $L_{36}FGSIFGGN_{44}$, is greatly reduced[9]. Interestingly, the binding affinity is enhanced and is comparable to TerD when the extra segment is deleted ($TerZ_{del}$). To better understand how the extra segment affects Ca^{2+}-binding affinity, we carried out several biophysical experiments on both TerZ and $TerZ_{del}$. We found that TerZ is easier to aggregate and thermally less stable than $TerZ_{del}$. Chemical shift index and homology modeling results indicated that the extra segment, forming an extended loop, may disturb the conformation of Ca^{2+}-binding sites and also prevent Ca^{2+} from its binding site, hence leading to the significantly reduced and weak Ca^{2+}-binding affinity of TerZ.

Fig. 1 Sequence alignment of TerZ (UniProt name: C4XDI9_KLEPN), TerD (C4XDJ3_KLEPN) and TerE (C4XDJ4_KLEPN) from *K. pneumoniae* is shown. Residues involved in the 2 Ca^{2+}-binding sites of TerD are indicated by filled (site 1) and opened (site 2) circles, respectively. The extra 9-residue segment ($L_{36}FGSIFGGN_{44}$) observed in TerZ are boxed with dash lines

1 Materials and methodology

1.1 Protein preparation of TerZ and $TerZ_{del}$

The DNA fragments encoding TerZ and $TerZ_{del}$, with L36 to N44 of TerZ deleted, were amplified from a *K. pneumoniae* NTUH-K2044 cDNA library[10] by PCR and cloned into the pET-29b vector (Novagen). The TerZ recombinant protein contains 194 amino acids, and both TerZ and $TerZ_{del}$ were constructed with 8 extra residues (LEHHHHHH) at the C-terminus and expressed in *E. coli* BL21 (DE3). For labeled (^{15}N, $^{15}N/^{13}C$ and $^{15}N/^{13}C/^{2}H$) proteins, the cells were grown in H_2O- or D_2O-containing M9 minimal medium containing $^{15}NH_4Cl$ (1 g/L) and/or ^{13}C-glucose (2 g/L) at 37 ℃ with 30 μg/mL kanamycin until OD_{600} = 0.5, then were induced with 1 mmol/L isopropyl-β-thiogalactopyranoside (IPTG) for 4 h. The cells were harvested and lysed in buffer (20 mmol/L Tris, pH 8.0, 500 mmol/L NaCl) by use of a microfluidizer (Microfluidics). The proteins were purified by nickel-nitrilotriacetic acid (Ni-NTA) affinity chromatography. Purity and authenticity of the recombinant proteins were verified by SDS-PAGE and mass spectrometry. Finally, the target proteins were dialyzed and concentrated with buffer [50 mmol/L NaH_2PO_4, 100 mmol/L NaCl, 0.5 mmol/L NaN_3, 1 mmol/L EDTA and 1 mmol/L Tris (2-carboxyethyl) phosphine hydrochloride (TCEP)] at pH 7.2 for NMR structural study.

1.2 Circular dichroism (CD) experiments

All CD spectra were collected on an Aviv CD 202 spectrometer (Lakewood, NJ) calibrated with (+)-10-camphorsulfonic acid. TerZ and $TerZ_{del}$ were prepared with 50 mmol/L sodium phosphate buffer at pH 7.2 or buffer with 1 mmol/L $CaCl_2$. The spectra were acquired at 25 ℃ with ~20 μmol/L protein samples in a 1 mm cuvette. The signals from 200 to 260 nm were recorded 3 times with a wavelength step of 0.5 nm and converted from CD signal (millidegree) into mean residue ellipticity after subtraction of the background signals. Thermal-denaturation experiments were obtained by measuring the change of CD signal at 215 nm from 24 ℃ to 98 ℃ with a 2 ℃ interval and 2 min for thermal equilibrium. The equilibrium thermal unfolding curves of TerZ proteins in various conditions were fitted by two-state model.

1.3 Analytical ultracentrifugation (AUC)

Sedimentation velocity (SV) experiments were performed using an XL-A analytical ultracentrifuge (Beckman Coulter, Fullerton, CA) with absorption optics in an An-60 Ti rotor with cells containing quartz windows. TerZ and $TerZ_{del}$ were diluted to a concentration of 14 μmol/L into phosphate buffer (50 mmol/L NaH_2PO_4, 100 mmol/L NaCl, 0.5 mmol/L NaN_3 and 1 mmol/L TCEP at pH 7.2) and buffer with 1 mmol/L $CaCl_2$ or 2 mmol/L EDTA. Samples and control reference buffer (~400 μL) were loaded into double-sector centerpieces and spun at 60 000 rpm at 20 ℃. The radial absorbance data at 280 nm was acquired at 3 min intervals. Buffer density and viscosity were calculated using SEDNTERP, and the data were analyzed using SEDFIT (version 14.1) software[11].

1.4 NMR experiments

NMR samples (^{15}N, $^{15}N/^{13}C$ and $^{15}N/^{13}C/^{2}H$ isotopically labeled proteins) at pH 7.2 in phosphate buffer were prepared. Each 0.6−1 mmol/L protein sample contained ~0.30 mL of 90% H_2O/10% D_2O solution in a Shigemi NMR tube. All NMR spectra were acquired with the use of a Bruker AVANCE 800 MHz spectrometer equipped with a triple (^{1}H, ^{13}C and ^{15}N) resonance cryoprobe, which included a shielded *z*-gradient at 298 K. The sequential backbone assignment was achieved by using HNCACB, HN(CO)CACB, and HNCO spectra of $TerZ_{del}$ and TROSY-HNCACB, TROSY-HN(CO)CACB, TROSY-HNCO and TROSY-HN(CA)CO spectra of TerZ. The ^{1}H side-chain resonances were assigned by HAHB(CO)NH, NOESY-HSQC and HCCH-COSY experiments. All spectra were processed by use of Bruker Topspin 3.0 (Karlsruhe, Germany) and NMRPipe[12], and data were analyzed by use of NMRView[13].

1.5 Homology Modeling

The solution structures of Ca^{2+}-bound TerD (PDB ID: 2KXV) was applied as a template to model the Ca^{2+}-bound TerZ by using three homology modeling methods, Discovery Studio v.4.0 (Accelrys Software Inc., USA), SWISS MODEL[14], and Modeller[15]. Furthermore, the models were examined by checking the stereochemical quality using Procheck program and Ramachandran plot[16,17].

2 Results and discussion

2.1 TerZ and $TerZ_{del}$ have similar secondary structures but with distinct stability

As shown in Fig. 2(a), CD spectra of TerZ and $TerZ_{del}$ in the absence of Ca^{2+} are well superimposed, indicating that the free TerZ and $TerZ_{del}$ possess very similar secondary structure. Besides, the spectra of Ca^{2+}-bound TerZ and $TerZ_{del}$ are almost superimposed either. However, the spectra between the free and bound forms apparently are different, revealing that there is conformational change between them. The T_m values measured by CD thermal-denaturation experiment [Fig. 2(b)] are 62.16 and 67.33 ℃ for the free and Ca^{2+}-bound TerZ, and 70.84 and 75.97 ℃ for the free and Ca^{2+}-bound $TerZ_{del}$, respectively. Clearly, the Ca^{2+}-bound form is more stable than the free form, and $TerZ_{del}$ has better thermal stability compared to TerZ. We also applied differential scanning fluorimetry to investigate the thermal stability on both TerZ and $TerZ_{del}$ proteins (data not shown), and the result is consistent with CD thermal-denaturation experiment.

2.2 Ca^{2+}-bound TerZ and $TerZ_{del}$ form oligomeric structure

We further characterized the structural properties on $TerZ_{del}$ and TerZ in free and Ca^{2+}-bound forms using AUC experiment [Fig. 3(a) and 3(b)]. The sedimentation coefficient distribution of the free $TerZ_{del}$ in phosphate buffer at pH 7.2 showed 2 peaks at 2.3 *s* and 3.2 *s*, respectively. The major one (2.3 *s*) corresponds to a molecular weight of ~22 k, indicative of the formation of monomer, and the minor one (3.2 *s*) is likely due to the formation of dimer. By contrast, the Ca^{2+}-bound $TerZ_{del}$ only showed a broad peak at 3.3 *s*, revealing that it

predominantly forms the dimer. We also found that the bound $TerZ_{del}$ treated with enough amount of EDTA only showed a single peak at 2.3 *s*, that is, in the monomeric form. TerZ exhibts similar results as seen in $TerZ_{del}$ except that the bound TerZ has the peak maximum at 5.1 *s*, which corresponds to a molecular weight of ~69 k, indicating the formation of trimer. Taken together, AUC data revealed that the free TerZ and $TerZ_{del}$ mainly form monomeric structures, while bound to Ca^{2+}, the oligomerization in TerZ (from monomer to trimer) and $TerZ_{del}$ (from monomer to dimer) were observed. Also, both TerZ and $TerZ_{del}$ with enough amount of EDTA can form a monomeric structure with high homogeneity.

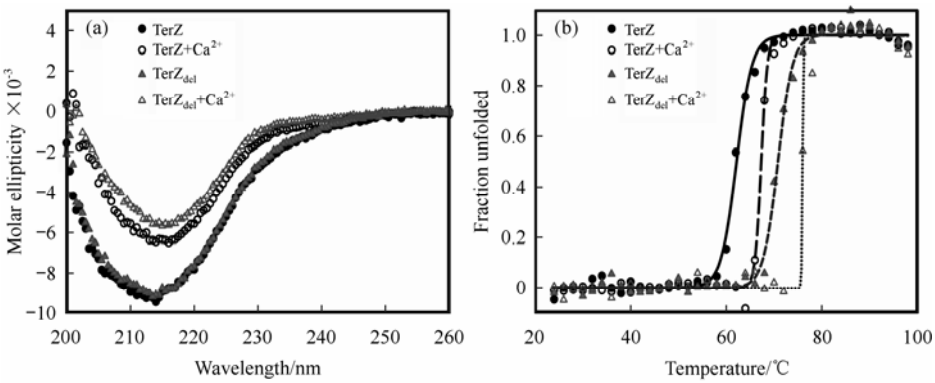

Fig. 2 (a) Comparison of CD spectra of TerZ and $TerZ_{del}$ in the presence and absence of Ca^{2+} at 25 ℃. (b) The equilibrium thermal-denaturation experiments of TerZ and $TerZ_{del}$ in both free and bound forms were acquired at 215 nm

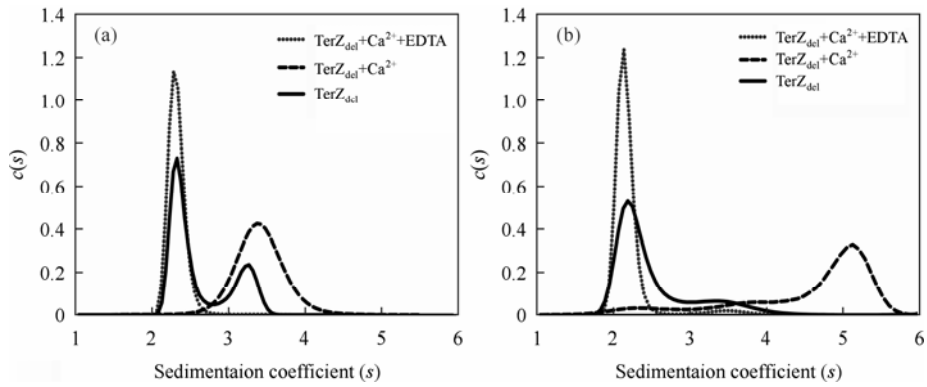

Fig. 3 Analysis of the Ca^{2+}-induced aggregation of $TerZ_{del}$ and TerZ using AUC experiments. Sedimentation coefficient distributions were calculated from sedimentation velocity experiments of $TerZ_{del}$ (a) and TerZ (b) in various conditions using a continuous *c*(*s*) distribution model

2.3 NMR assignment and secondary structure

The well-superimposed 2D ^{1}H-^{15}N HSQC spectra revealed that the free TerZ and $TerZ_{del}$ have similar structures, in good agreement with CD result. Based on the 3D

triple-resonance experiments, we finished the backbone and side-chain $^{13}C_{\beta}$ assignments for all residues except V2, F117, R131 and I180 on TerZ [Fig. 4(a)]. The unassigned residues are presumably due to fast amide-proton exchange rate with H_2O. Unusual chemical shifts were observed for 2 backbone amide protons, R69 (δ 3.9) and G82 (δ 11.5). Interestingly, these unusual chemical shifts were also observed in the Ca^{2+}-bound TerD (BMRB accession No. 16929), and were identified to be due to hydrogen bond formation and ring current effect, respectively. Neither TerZ nor $TerZ_{del}$ in the Ca^{2+}-bound form could obtain a well-dispersed ^{1}H-^{15}N HSQC spectra [Fig. 4(b) and 4(c)] because as concluded in AUC result they form

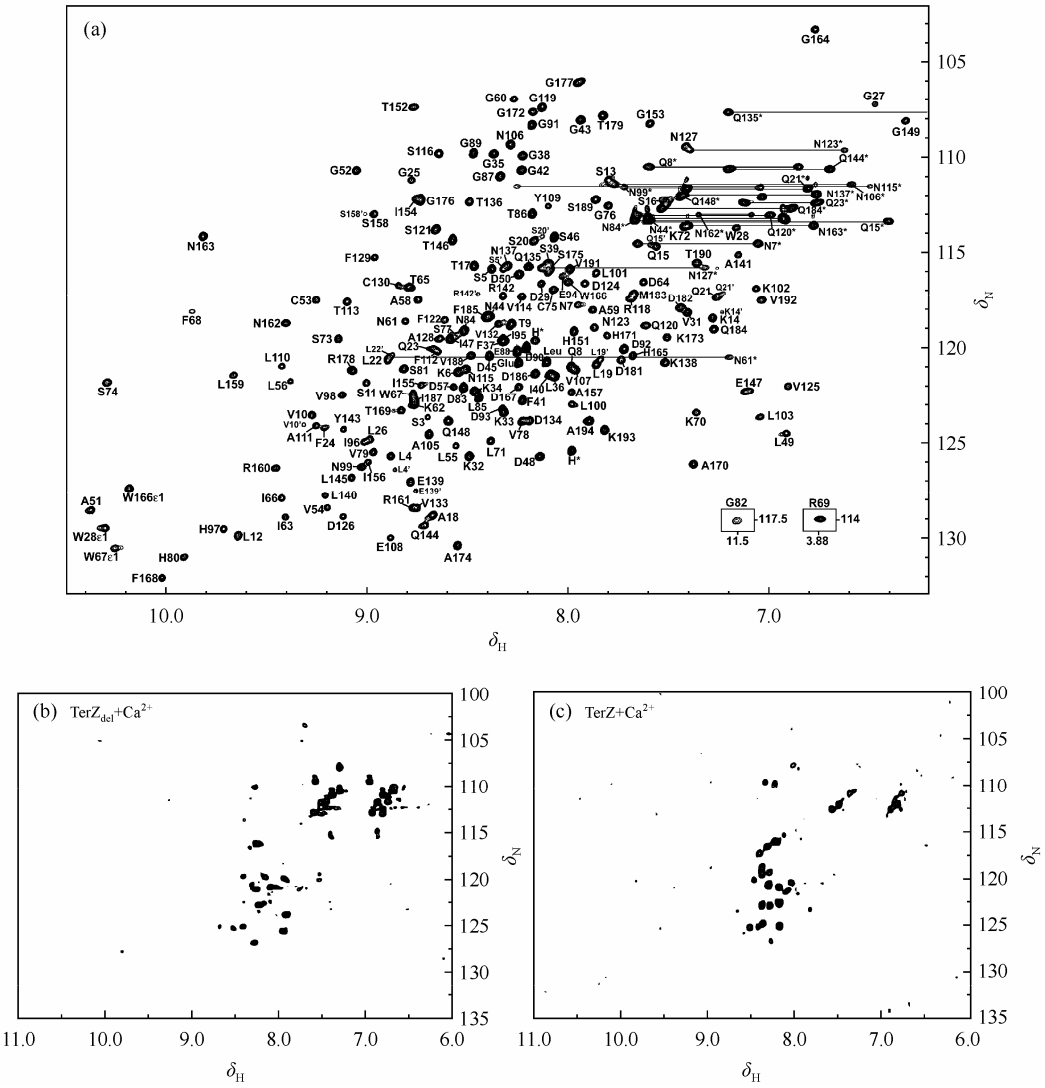

Fig. 4 (a) ^{1}H-^{15}N HSQC spectrum of the free TerZ acquired at 298 K on a Bruker AVANCE 800 MHz spectrometer is shown. The assignments of the side-chain amide protons of Asn and Gln are linked by horizontal lines and labeled with an asterisk. ^{1}H-^{15}N HSQC spectra of Ca^{2+}-bound $TerZ_{del}$ (b) and Ca^{2+}-bound TerZ (c) acquired in the same condition as for free TerZ

oligomeric structures. The predicted secondary structure by TALOS-N[18] with a combination of 6 kinds (^{15}N, $^{1}H_N$, $^{1}H_\alpha$, $^{13}C_\alpha$, $^{13}C'$ and $^{13}C_\beta$) of chemical shift assignments showed that the free TerZ is mainly composed of 4 α-helices and 12 β-strands, and the extra 9-residue segment is unstructured (Fig. 5). Compared to the Ca^{2+}-bound TerD structure, the main structural differences between the free TerZ and the bound TerD are at the N-terminal 18 residues, residues N61−I66 and Q144−G149, which may be the key regions, causing structural changes from the free to the bound form for tellurite resistance proteins, such as TerD, TerZ, etc. The ^{1}H, ^{13}C, and ^{15}N chemical shifts of the free TerZ have been deposited in the BioMagResBank (http://www.bmrb.wisc.edu; BMRB accession No. 19706).

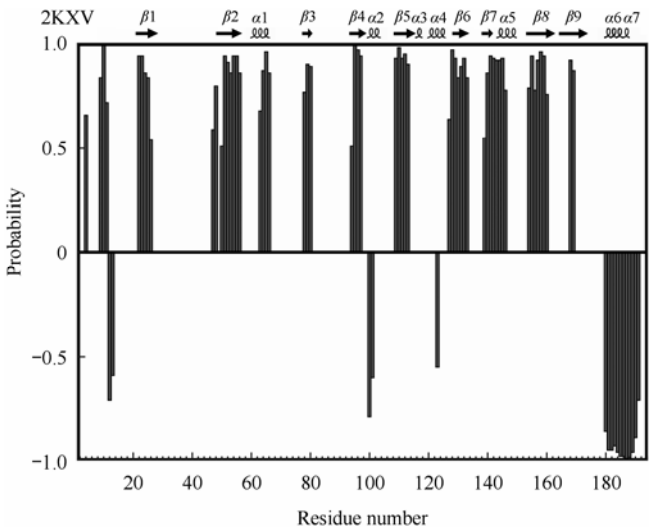

Fig. 5 The predicted secondary structure elements are displayed by TALOS-N. Residues having a probability of at least 0.5 are shown, with negative and positive bars indicating α-helix and β-strand, respectively. The corresponding regions of the secondary structures seen in the Ca^{2+}-bound TerD solution structure are displayed on the top of the Figure

2.4 Homology structure

We have built the structural model of Ca^{2+}-bound TerZ by molecular modeling programs, Discovery Studio v.4.0 (Accelrys Software Inc., USA), SWISS MODEL, and Modeller, using the structure of Ca^{2+}-bound TerD (PDB ID: 2KXV) as a template. The built models were further evaluated by Procheck program and Ramachandran plot to check the stereochemical quality. The results showed that the residues in the disallowed regions of the constructed models by Discovery Studio v.4.0, SWISS MODEL, and Modeller are 0, 2.1 and 1.8%, respectively (data not show). Therefore, the model built by Discovery Studio v.4.0 was chosen for further analysis. Structural comparison of the Ca^{2+}-bound TerD and TerZ (Fig. 6) obviously showed that the extra 9-residue segment of TerZ actually forms an extended loop, greatly enhancing the loop length so that this extended loop is much more flexible than the

corresponding loop in TerD.

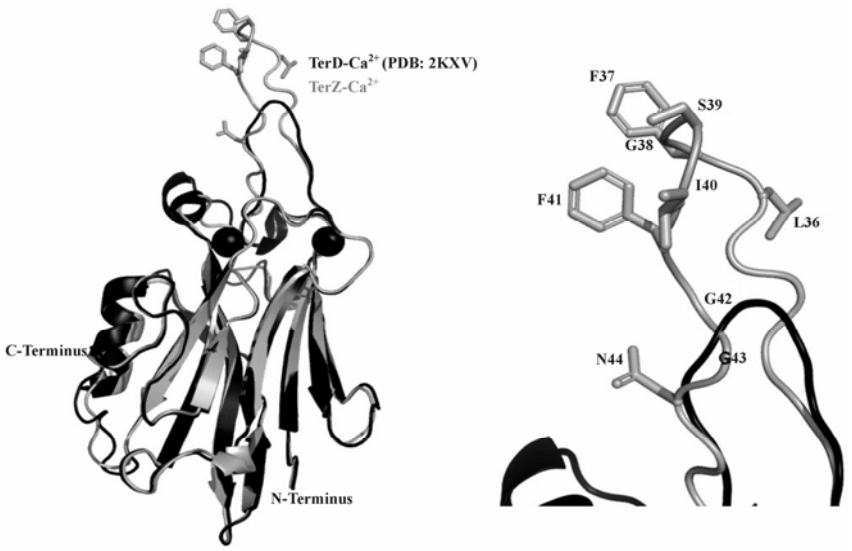

Fig. 6 The homology model of the Ca^{2+}-bound TerZ. The left panel is the model of Ca^{2+}-bound TerZ (colored in gray) superimposed with the structure of the Ca^{2+}-bound TerD (PDB ID: 2KXV, colored in black), *RMSD* = 0.3 nm. 2 Ca^{2+} ions are shown as spheres and the extra 9-residue loop (L_{36}FGSIFGGN_{44}) are presented as sticks. The right panel shows the zoom-in view of the extra 9-residue loop of the Ca^{2+}-bound TerZ

3 Conclusion

Previously, based on EDTA titrations we found by one-dimensional NMR that the native TerZ has much weaker Ca^{2+}-binding affinity than TerD, and interestingly, $TerZ_{del}$ has comparable binding affinity. CD and NMR data clearly revealed that the free TerZ and $TerZ_{del}$ have very similar secondary and tertiary structures. Some residues (W28, D48, L49, D50, D83, N84) corresponding to the Ca^{2+}-binding residues of TerD and their adjacent residues (G27, D29, I47, A51, G82, D85) shifted in the superimposed HSQC spectra of TerZ and $TerZ_{del}$ (Fig. 7). The extra 9-residue segment observed in TerZ apparently not only extends the loop length, which hence significantly enhances loop flexibility, but also perturbs Ca^{2+}-binding sites. We suggested that this extended loop may disturb the conformation of Ca^{2+}-binding sites and also prevent Ca^{2+} to access the binding sites due to its high flexibility, both of which could reduce Ca^{2+} binding ability on TerZ. In addition, the Ca^{2+}-bound TerZ is less thermally stable and easier to form aggregation than the Ca^{2+}-bound $TerZ_{del}$, which may provide valuable information for better understanding the biological role and action that TerZ plays in physiological condition (*in vivo*).

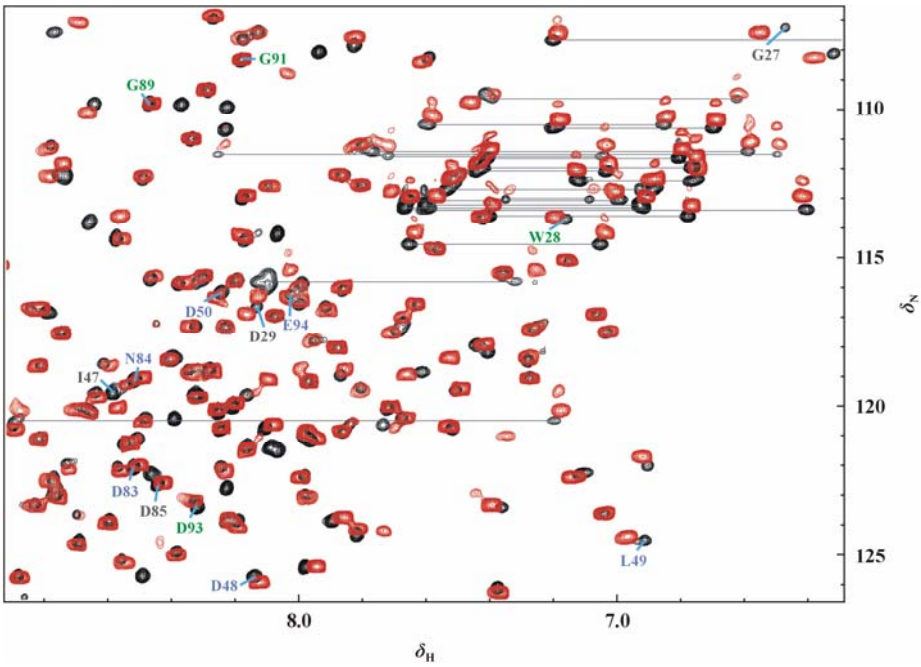

Fig. 7 The overlaid ^{1}H-^{15}N HSQC spectra of the free TerZ (black) and $TerZ_{del}$ (red). Residues of TerZ corresponding to 2 Ca^{2+}-binding sites of TerD are labeled in blue (site 1) and green (site 2), respectively

Acknowledgement: This work was supported by "Academia Sinica and the National Science Council (NSC103-2311-B-001-026-MY3)", Taiwan. The NMR spectra were obtained at the High-field Biomacromolecular NMR Core Facility at "Academia Sinica", which is supported by "the National Science and Technology Program" for Medical Genomics. The use of CD and AUC were provided from the Biophysics Core Facility, Scientific Instrument Center at "Academia Sinica".

Reference:

[1] Taylor D E. Bacterial tellurite resistance[J]. Trends Microbiol, 1999, 7(3): 111－115.

[2] Chasteen T G, Fuentes D E, Tantalean J C, *et al*. Tellurite: history, oxidative stress, and molecular mechanisms of resistance[J]. FEMS Microbiol Rev, 2009, 33(4): 820－832.

[3] Walter E G, Taylor D E. Plasmid-mediated resistance to tellurite: expressed and cryptic[J]. Plasmid, 1992, 27(1): 52－64.

[4] Chen Y T, Chang H Y, Lai Y C, *et al*. Sequencing and analysis of the large virulence plasmid pLVPK of *Klebsiella pneumoniae* CG43[J]. Gene, 2004, 337: 189－198.

[5] Whelan K F, Colleran E, Taylor D E. Phage inhibition, colicin resistance, and tellurite resistance are encoded by a single cluster of genes on the IncHI2 plasmid R478[J]. J Bacteriol, 1995, 177(17): 5 016－5 027.

[6] Valkovicova L, Vavrova S M, Mravec J, *et al*. Protein-protein association and cellular localization of four essential gene products encoded by tellurite resistance-conferring cluster "ter" from pathogenic *Escherichia coli*[J]. Antonie Van Leeuwenhoek, 2013, 104(6): 899－911.

[7] Anantharaman V, Iyer L M, Aravind L. Ter-dependent stress response systems: novel pathways related to metal sensing, production of a nucleoside-like metabolite, and DNA-processing[J]. Mol Biosyst, 2012, 8(12): 3 142－3 165.

[8] Pan Y R, Lou Y C, Seven A B, *et al*. NMR structure and calcium-binding properties of the tellurite resistance protein TerD from *Klebsiella pneumoniae*[J]. J Mol Biol, 2011, 405(5): 1 188－1 201.

[9] Pan Y R. Structure as a Guide to Function: NMR Studies on Tellurite Resistance Proteins from Klebsiella pneumoniae[D]. Hsinchu: Institute of Bioinformatics and Structural Biology, College of Life Science, “National Tsing Hua University”, 2011.

[10] Wu K M, Li L H, Yan J J, *et al*. Genome sequencing and comparative analysis of *Klebsiella pneumoniae* NTUH-K2044, a strain causing liver abscess and meningitis[J]. J Bacteriol, 2009, 191(14): 4 492－4 501.

[11] Schuck P. Size-distribution analysis of macromolecules by sedimentation velocity ultracentrifugation and lamm equation modeling[J]. Biophys J, 2000, 78(3): 1 606－1 619.

[12] Delaglio F, Grzesiek S, Vuister G W, *et al*. NMRPipe: a multidimensional spectral processing system based on UNIX pipes[J]. J Biomol NMR, 1995, 6(3): 277－293.

[13] Johnson B A, Blevins R A. NMR View: A computer program for the visualization and analysis of NMR data[J]. J Biomol NMR, 1994, 4(5): 603－614.

[14] Biasini M, Bienert S, Waterhouse A, *et al*. SWISS-MODEL: modelling protein tertiary and quaternary structure using evolutionary information[J]. Nucleic Acids Res, 2014, 42(W1): W252－W258.

[15] Sali A, Blundell T L. Comparative protein modelling by satisfaction of spatial restraints[J]. J Mol Biol, 1993, 234(3): 779－815.

[16] Morris A L, MacArthur M W, Hutchinson E G., *et al*. Stereochemical quality of protein structure coordinates[J]. Proteins, 1992, 12(4): 345－364.

[17] Laskowski R A, Macarthur M W, Moss D S, *et al*. Procheck: a program to check the stereochemical quality of protein structures[J]. J Appl Cryst, 1993, 26(0), 283－291.

[18] Shen Y, Bax A. Protein backbone and sidechain torsion angles predicted from NMR chemical shifts using artificial neural networks[J]. J Biomol NMR, 2013, 56(3): 227－241.

克雷伯氏肺炎杆菌内抗亚碲酸盐蛋白质 TerZ 延伸环降低对钙离子亲合性

魏淑怡，潘韻如，曾天生，陈金榜*

（“中央研究院”生物医学科学研究所，台北 11529）

摘　要：亚碲酸盐是碲的一含氧阴离子，其对微生物具高度毒性．在许多的致病菌内已经鉴定出数个抗亚碲酸盐基因(*terZABCDEF*)．之前，作者解出抗亚碲酸盐蛋白质 TerD 液体核磁共振结构并指出在细菌内 TerD 可能是一钙离子传感器．TerZ 与 TerD 在序列上有 40%相同性，其包括了一额外的 9 氨基酸片段 L36–N44，并且显示出非常弱的钙离子亲合性．有趣的是，少了额外片段的 $TerZ_{del}$ 拥有与 TerD 可比较的钙离子亲合性．根据化学位移指数及同源模拟结果，此额外片段为一无二级结构且延伸的 loop，可能扰乱钙离子结合位置的构形，同时也阻碍了钙离子接近其结合位置，因此大大降低钙离子亲合性．

关键词：钙离子结合蛋白质；抗亚碲酸盐；钙离子传感器；化学位移指数；同源模拟

*通讯联系人：陈金榜，电话：+886-2-27899162, E-mail: bmchinp@ibms.sinica.tw.